Formation and electronic structure of an atypical Cu_A site

Journal:	*Journal of the American Chemical Society*
Manuscript ID	ja-2018-13610d.R1
Manuscript Type:	Article
Date Submitted by the Author:	22-Feb-2019
Complete List of Authors:	Ross, Matthew; Northwestern University, Chemistry Fisher, Oriana; Northwestern University, Molecular Biosciences Morgada, Marcos; Instituto de Biologia Molecular y Celular de Rosario, Metalloproteins Lab Krzyaniak, Matthew; Northwestern University, Chemistry Wasielewski, Michael; Northwestern University, Department of Chemistry Vila, Alejandro J.; Universidad Nacional de Rosario - CONICET, IBR (Instituto de Biologia Molecular y Celular de Rosario) Hoffman, Brian; Northwestern University, Chemistry Rosenzweig, Amy; Northwestern University, Molecular Biosciences

Formation and electronic structure of an atypical Cu_A site

Matthew O. Ross,[†,‡,§] Oriana S. Fisher,[†,‡,§] Marcos N. Morgada,[#,¶] Matthew D. Krzyaniak,[∥] Michael R. Wasielewski,[∥] Alejandro J. Vila,[#] Brian M. Hoffman,[*,†,‡] Amy C. Rosenzweig[*,†,‡]

[†]Departments of Molecular Biosciences and of [‡]Chemistry, Northwestern University, Evanston, IL, USA. [*]E-mail: bmh@northwestern.edu, amyr@northwestern.edu.

[#]Instituto de Biología Molecular y Celular de Rosario (IBR, CONICET-UNR), Ocampo y Esmeralda, S2002LRK Rosario, Argentina.

[¶]Área Biofísica, Facultad de Ciencias Bioquímicas y Farmacéuticas, Universidad Nacional de Rosario, S2002LRK Rosario, Argentina.

[∥]Department of Chemistry and Institute for Sustainability and Energy at Northwestern, Northwestern University, 2145 Sheridan Rd, Evanston, IL 60208, USA

Supporting Information Placeholder

ABSTRACT: PmoD, a recently discovered protein from methane-oxidizing bacteria, forms a homodimer with a dicopper Cu_A center at the dimer interface. Although the optical and electron paramagnetic resonance (EPR) spectroscopic signatures of the PmoD Cu_A bear similarities to those of canonical Cu_A sites, there are also some puzzling differences. Here we have characterized the rapid formation (seconds) and slow decay (hours) of this homodimeric Cu_A site to two mononuclear Cu^{2+} sites, as well as its electronic and geometric structure, using stopped-flow optical and advanced paramagnetic resonance spectroscopies. PmoD Cu_A formation occurs rapidly and involves a short-lived intermediate with λ_{max} of 360 nm. Unlike other Cu_A sites, the PmoD Cu_A is unstable, decaying to two type 2 Cu^{2+} centers. Surprisingly, nuclear magnetic resonance (NMR) data indicate that the PmoD Cu_A has a pure σ_u* ground state (GS) rather than the typical equilibrium between σ_u* and π_u of all other Cu_A proteins. EPR, ENDOR, ESEEM, and HYSCORE data indicate the presence of two histidine and two cysteine ligands coordinating the Cu_A core in a highly symmetrical fashion. This report significantly expands the diversity and understanding of known Cu_A sites.

INTRODUCTION

Biological copper centers play key roles in many enzymes and proteins, both catalyzing chemical reactions and mediating electron transfer (ET). Dicopper Cu_A centers are ET sites found in enzymes such as cytochrome *c* oxidase (C*c*O) and nitrous oxide reductase (N_2OR), which are terminal electron acceptors for aerobic and anaerobic respiration, respectively.[1] Initially a source of controversy,[2] Cu_A sites are now well known to contain a $Cu_2[S(Cys)]_2$ core with two Cu ions bridged by two Cys side chains as well as one in-plane His side chain ligand per Cu. In addition, there is a weak axial Met side chain ligand on one Cu and an axial backbone carbonyl oxygen ligand on the other that induce a degree of structural asymmetry at the metal site. During ET, a Cu_A site cycles between the reduced $[2Cu]^{2+}$ and oxidized $[2Cu]^{3+}$ (often stylized as $Cu^{1.5+}$-$Cu^{1.5+}$ to reflect the electronic equivalence of the two Cu ions) states as it shuttles an electron to a metallocofactor.[1,3] The amino acid ligands to the C*c*O and N_2OR Cu_A sites are found in a $Hx_{34}Cx_3Cx_3Hx_2M$ motif,[2] derived from a single polypeptide with a cupredoxin fold.[4-6]

We recently discovered a new type of Cu_A site in some homologs of PmoD/AmoD, a protein encoded exclusively in the genomes of methane- and ammonia-oxidizing bacteria.[7] This Cu_A forms in PmoD proteins encoded within methanotroph *pmo* operons. These operons also contain the genes encoding the three subunits of particulate methane monooxygenase (pMMO),[7] a copper-dependent integral membrane enzyme that converts methane to methanol.[8] In *Methylosinus trichosporium* OB3b, the *pmoD* gene in the *pmo* operon is co-regulated with the pMMO genes,[9] and its disruption results in a severe copper-dependent growth defect.[7] Biochemical, structural, and spectroscopic data indicate that the N-terminal periplasmic domain of PmoD from *Methylocystis* species strain Rockwell adopts a cupredoxin-like fold and forms a mixed-valence, delocalized $Cu_2[S(Cys)]_2$ Cu_A core at the interface of a PmoD homodimer utilizing a Cx_7MxH binding motif rather than the typical Cu_A $Hx_{34}Cx_3Cx_3Hx_2M$ motif (Figure 1A). In contrast to canonical Cu_A sites, each PmoD monomer is proposed to

contribute one Cys41 ligand to the $Cu_2[S(Cys)]_2$ core as well as one Met49 and one His51 from each Cx_7MxH motif. Mutation of these residues prevents Cu_A formation, and the Cx_7MxH motif is highly conserved in PmoD homologs from *pmo* operons in alpha-proteobacterial methanotrophs.[7]

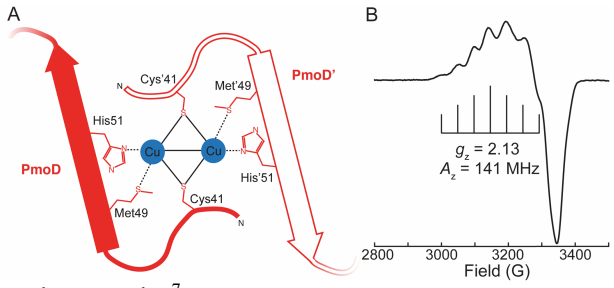

Figure 1. The PmoD Cu_A site. (A) Homodimeric molecular model. (B) CW X-band (~9.5 GHz) EPR spectrum of the PmoD Cu_A. Bracket defines the hyperfine splitting A_z (adapted from [7]).

Copper-loaded PmoD exhibits an electron paramagnetic resonance (EPR) spectrum with a seven hyperfine-line splitting (A_z) along g_z,[7] defining its Cu_A as a Robin-Day class III fully valence-delocalized $[2Cu]^{3+}$ dicopper center (Figure 1B). Similar to other Cu_A sites, the PmoD g_z and A_z values are less than those observed for "normal" type 2 monocopper sites, in part due to the highly covalent Cu-S(Cys) bonding, which leads to very large $\rho_{S(Cys)}$ (where ρ_X is the spin density on atom X) and small ρ_{Cu} (for example, for Cu_AAz, total $\rho_{S(Cys)}$ = 46%, total ρ_{Cu} = 44%).[10,11] The PmoD optical spectrum is dominated by the two typical S(Cys)-Cu ligand-to-metal charge transfer (LMCT) bands at 475 and 530 nm and a $\psi \rightarrow \psi^*$ intervalence band in the near-IR (770 nm).[7] The intensity of these LMCT bands is consistent with large Cu-S(Cys) covalence that gives rise to a large $\rho_{S(Cys)}$. The energy of the near-IR optical transition of a Cu_A center is inversely correlated with the Cu-Cu distance and reflects the relative strength of the Cu-Cu and Cu-N(His) bonds; a high energy transition corresponds to strong Cu-Cu and Cu-N(His) bonding.[12-14] The PmoD near-IR optical transition is blue-shifted with respect to those observed for *Pseudomonas nautica* N_2OR (*Pn*N_2OR, 800 nm)[15] and *Thermus thermophilus* C*c*O (*Tt*C*c*O, 790 nm),[16] and is comparable to that reported for the semisynthetic Cu_A-containing azurin (Cu_AAz, 765 nm).[17] This shift suggests strong Cu-Cu bonding in PmoD, consistent with the short Cu-Cu distance determined from extended X-ray absorption fine structure (EXAFS) data (2.41 Å for PmoD, compared to 2.43 Å for *Tt*C*c*O, 2.43 Å for *Pn*N_2OR, and 2.39 Å for Cu_AAz).[7,14,18,19]

However, a variety of the characteristics of the PmoD Cu_A are not typical for a Cu_A center. The energy of the near-IR transition is highly sensitive to the Cu_A electronic structure and resulting spin density distribution, and Cu_A proteins with similar near-IR transition energies typically have similar EPR spectra.[12,13,20] Although the energies of the near-IR transitions of Cu_A-containing PmoD and Cu_AAz are essentially the same, their Cu hyperfine couplings are appreciably different (PmoD A_z = 141 MHz; Cu_AAz A_z = 167 MHz).[7,14] The Cu_A A_z is proportional to ρ_{Cu},[21] and thus the decreased PmoD Cu_A A_z value indicates anomalously small ρ_{Cu}, and by extension, correspondingly large spin density on the ligands. Likewise, another PmoD spin-Hamiltonian parameter, g_z, has the smallest value of any Cu_A site (PmoD g_z = 2.13, Cu_AAz g_z = 2.17, and SoxM g_z = 2.20 (the largest g_z for a biological Cu_A)).[1,7,14,22]

To understand the unusual spectroscopic characteristics of the PmoD Cu_A site and to gain insight into its possible functions, we have studied its rapid (seconds) formation as Cu^{2+} is added to PmoD, and its subsequent slow decay (hours) to two mononuclear Cu^{2+} sites. We additionally probed the electronic and geometric structure of the PmoD Cu_A by nuclear magnetic resonance (NMR) and advanced paramagnetic resonance spectroscopies: EPR, electron nuclear double resonance (ENDOR), electron spin echo modulation (ESEEM), and hyperfine sublevel correlation (HYSCORE).

EXPERIMENTAL SECTION

Expression and purification of PmoD. The periplasmic domain of *Methylocystis sp.* str. Rockwell PmoD encoded within the *pmo* operon (locus tag Met49242_1452) was expressed in *E. coli* BL21* using the N-terminally His_6-tagged constructs for the wildtype (WT) and Cys65Ser proteins and purification protocols described previously.[7] Briefly, cells were grown in autoinduction media and harvested after overnight incubation. The cell pellets were resuspended in a lysis buffer composed of 20 mM imidazole, 20 mM Tris, pH 8, 500 mM NaCl, 1 mM DTT, 1 mg/mL DNaseI, and 1 mM PMSF. After lysis by sonication, cell debris was removed by centrifugation and the clarified lysate was purified on NiNTA resin. The His_6 tag was then removed by overnight incubation with His-tagged TEV protease. After removal of the TEV protease using a second NiNTA column, the untagged PmoD was stored in 20 mM Tris, pH 7.0 and 1 mM DTT. The protein concentrations of all PmoD samples were determined by the Bradford assay using known concentrations of BSA to generate a standard curve.

Stopped-flow optical spectroscopy. All stopped-flow experiments were conducted on a SX20 stopped-flow instrument (Applied Photophysics) at 6 °C. Purified PmoD samples were diluted to 200 µM in 20 mM Tris pH 7.5, 100 mM NaCl and loaded into one syringe. The second syringe was loaded with 400 µM $CuSO_4$. To obtain full kinetic spectra for each sample, a photodiode array (PDA) detector was used to collect 1000 data points logarithmically over a 1000 s time interval. The rates of formation and decay of the Cu_A species were calculated using the data from these experiments at 475 nm. To determine the rates for the 360 nm intermediate, a PMT detector was

used to allow for collection of sufficient data at the earliest time points. In these experiments, 1000 data points were collected logarithmically over a 5 s time interval. For the Cys65Ser variant, which exhibited slower kinetics for formation of the 360 nm species, data were collected over a 20 s time interval. Kinetic data were analyzed using GraphPad Prism.

Preparation and analysis of samples to monitor decay of the Cu_A site. For both the WT and Cys65Ser samples, the DTT-reduced protein was buffer exchanged into 20 mM Tris, pH 7.5, 100 mM NaCl. Two molar equivalents of $CuSO_4$ were slowly added to the protein by pipetting. Unbound copper was removed immediately by loading the sample onto a PD10 desalting column (GE), eluting into 20 mM Tris, pH 7.5, 100 mM NaCl, and concentrating to 150 μM using a 10 kDa molecular weight cut-off centrifugal concentrator (Millipore). Samples were stored on ice and removed at specific time points ranging from 0 to 144 hr for further analysis by optical and X-band continuous wave (CW) EPR spectroscopy as well as inductively coupled plasma optical emission spectroscopy (ICP-OES). X-band EPR samples were prepared by transferring ~180 μL of protein solution to a Wilmad quartz EPR tube (Sigma Aldrich), which was then frozen in liquid nitrogen, where it was stored until analysis. Optical spectra were collected at room temperature on 100 μL protein in a quartz cuvette (Helma) using an Agilent 8453 spectrophotometer. Prior to conducting elemental analysis, each protein sample was first applied to a PD-10 column and eluted into 20 mM Tris, pH 7.5, 100 mM NaCl to ensure that the copper was not dissociating from the protein through the timecourse. The protein was then digested in 5% nitric acid in metal-free conical tubes (VWR). A dilution series of a custom multi-element standard (Inorganic Ventures) was also prepared in a similar fashion to generate a standard curve. The copper contents of the samples were determined by ICP-OES using a Thermo iCAP 7600 instrument in the Quantitative Bioelement Imaging Center (QBIC) core facility at Northwestern University.

Oligomerization analysis of PmoD pre- and post-EDTA treatment. DTT-treated Cys65Ser PmoD was exchanged into reductant-free buffer prior to the addition of two molar equivalents of $CuSO_4$. Excess copper was then removed by desalting on a PD10 column into 4 mL copper-free buffer. A 1 mL aliquot of this sample was immediately run on a Superdex 75 Increase column (GE). A second 1 mL aliquot was treated with 50 mM EDTA, pH 8 and incubated on ice for 3 hr prior to running on the Superdex 75 Increase column. The remaining sample was incubated on ice at 4 °C for 144 hr to allow the Cu_A site to decay and subjected to size exclusion chromatography and EDTA treatment as described for the earlier time points. The peak fractions from each column were pooled and concentrated using 10 kDa molecular weight cut-off centrifugal concentrators (Millipore). Approximately 60 μg of each sample was run on a denaturing gel in either the absence or presence of β-mercaptoethanol, and ICP-OES was used to confirm that the EDTA treatment effectively removed copper. The Cys41Ser/Cys65Ser sample was prepared as described for the Cys65Ser sample, and approximately 60 μg was run on a denaturing gel in the presence or absence of β-mercaptoethanol.

NMR spectroscopy. ^{1}H NMR spectra were recorded on a Bruker Avance II-600 NMR spectrometer. PmoD prepared in 100 mM NaCl, 20 mM Tris, pH 7.0 and 1 mM DTT was lyophilized using a FreeZone 4.5 Liter Cascade Benchtop Freeze Dry System (Keck Biophysics Facility, Northwestern University). Lyophilized samples of PmoD were dissolved in ultrapure water with 2 mM TCEP. $CuSO_4$ was added to form the PmoD Cu_A site and excess copper was removed by desalting using PD minitrap desalting columns pre-equilibrated with 100 mM phosphate buffer, 100 mM KCl, 10% D_2O, pH 7.2 before the acquisition. 16384 free induction decays were acquired with the use of a super-WEFT pulse sequence[23] (inter-pulse delay: 100 ms; accumulation: 1024 points; spectral width: 200 ppm), Fourier transformed with the use of an exponential window (LB = 150 Hz), and baseline corrected using TopSpin NMR Software.

EPR, ESEEM, and ENDOR spectroscopy. For the advanced spectroscopic studies of the PmoD Cu_A site, the Cu_A-containing dimeric species was isolated by size exclusion chromatography as described previously.[7] This sample was concentrated to 300 μM in 20 mM Tris, pH 7.0 and frozen in an X-band EPR tube. The sample was subsequently thawed on ice, and an aliquot was quickly transferred to a Q-band tube for Q-band measurements, after which point both EPR tubes were frozen in liquid nitrogen. X- and Q-band samples utilized Wilmad quartz EPR tubes (Sigma Aldrich) and custom quartz Q-band tubes, respectively. X-band EPR tubes were filled with ~180 μL of protein solution, while Q-band EPR tubes were filled with ~80 μL of protein solution. Samples were frozen in liquid nitrogen, where they were stored until analysis. All CW X-band EPR measurements were collected using a Bruker ESP-300 spectrometer with a liquid helium flow Oxford Instruments ESR-900 cryostat. All wide scan (2400-3600 G) spectra were background corrected by subtraction of an EPR spectrum of 50 mM Tris, pH 8.0, 150 mM NaCl measured under identical conditions. For Cu^{2+} spin quantitation, the double integral of the experimental spectrum was compared to that of Cu^{2+}-EDTA standards in 50 mM Tris, pH 8.0, 150 mM NaCl buffer containing 100-400 μM Cu^{2+}.

X-band three pulse [π/2–τ–π/2–T–π/2–τ–echo] ESEEM and four pulse [π/2–τ–π/2–T1 π/2–T2–π/2–τ–echo] HYSCORE measurements were collected on a Bruker Elexsys E580-X utilizing split ring resonator (ER4118X-MS5). The temperature was maintained at 10 K using an Oxford Instruments CF935 continuous flow cryostat using liquid helium.

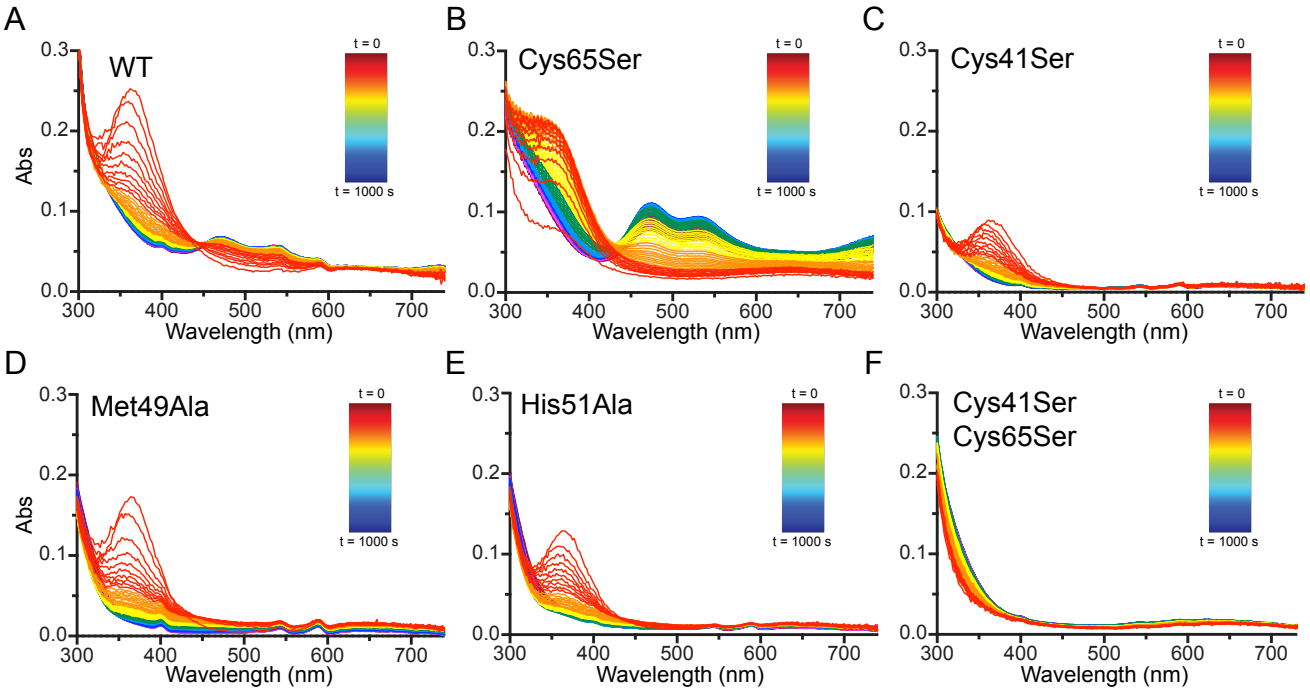

Figure 2. Stopped-flow optical spectroscopy experiments monitoring formation of the PmoD Cu_A site at room temperature. The optical spectra were monitored over 1000 s after mixing 400 μM $CuSO_4$ with 200 μM PmoD for (A) WT protein, (B) Cys65Ser variant, (C) Cys41Ser variant, (D) Met49Ala variant, (E) His51Ala variant, and (F) Cys41Ser/Cys65Ser variant. Red, 0.014 s-1.009 s; orange, 1.168-3.295 s; yellow, 3.634 s-8.183 s; green, 8.908 s-18.638 s; light blue, 20.184 s-40.976 s; blue, 44.29 s-190.867 s; purple, 206.014 s-409.204 s; dark purple, 441.588 s-1000 s.

Pulsed Q-band EPR, ENDOR, and PESTRE measurements were conducted at ~2 K in a liquid helium immersion dewar on a spectrometer described elsewhere, with SpinCore PulseBlaster ESR_PRO 400MHz digital word generator and Agilent Technologies Acquiris DP235 500 MS/sec digitizer using SpecMan software.[24,25] A Davies [π–T_{RF}–$\pi/2$–τ–π–τ–echo] pulse sequence was employed for all ENDOR measurements, in which T_{RF} denotes the interval during which the RF was applied.

RESULTS

Formation of the PmoD Cu_A center. To probe formation of the PmoD Cu_A site, we monitored the reaction between reduced PmoD and Cu^{2+} by stopped-flow optical spectroscopy. Cu_A formation is preceded by the development of a transient intermediate characterized by an intense absorbance feature at 360 nm, consistent with a S(Cys) to Cu^{2+} LMCT transition (Figure 2A).[26] The rate of formation for this intermediate is 660 s^{-1} and its rate of decay is 2.2 s^{-1} (Table S1). The rate of Cu_A formation (monitored at 475 nm; absorption bands at 475, 530, and 770 nm are characteristic of the Cu_A site) is similar to the rate of intermediate decay (Table S1). As the two share an isosbestic point, the 360 nm species directly converts to Cu_A. This mechanism resembles that observed for Cu_AAz and *T. thermophilus* cytochrome ba_3 Cu_A, wherein the "capture complex" type 2 'red' Cu^{2+} center, with λ_{max} ~ 385 nm, converts into the Cu_A center,[1,27] although the PmoD intermediate forms and decays on significantly shorter timescales and does not proceed through any of the additional intermediates observed in the other Cu_A systems.[27-29] As the stopped-flow optical spectroscopy experiment involves adding Cu^{2+} to form a mixed valent, formally Cu^{2+}-Cu^{1+} delocalized center, either or both of the cysteines in PmoD must be reducing Cu^{2+} to Cu^{1+} (with concomitant oxidation of cysteines to cystine). This Cu^{1+} is then used to produce the Cu_A as in other Cu_A metalation mechanisms.[27-29]

In the Cu_AAz mechanism, a solvent exposed cysteine first binds Cu^{2+} to form the 'red' Cu_{2+} intermediate and positions it for eventual Cu_A formation (a methionine was also proposed to be a ligand to this intermediate in the *T. thermophilus* cytochrome ba_3 Cu_A).[29] To determine whether this also occurs in PmoD and to identify which cysteine residue(s) may bind Cu^{2+} initially, we monitored Cu_A formation by variants lacking either or both cysteine residues. The Cys65Ser PmoD variant (a variant with the only non-Cu_A-ligating cysteine replaced with serine) also forms a 360 nm species which directly converts to Cu_A (Figure 2B), but the rate of intermediate formation is decreased nearly 100-fold compared to wild-type (WT) PmoD, while the rate of intermediate decay and Cu_A formation are very close. Furthermore, more of the Cu_A species is formed relative to WT despite a lower intensity 360 nm intermediate absorbance (Table S1, Figure 2B). By contrast, the Cys41Ser variant does not form the Cu_A site (Figure 2C), though it does still form a transient 360 nm intermediate with similar

kinetics to WT PmoD (Table S1). These results suggest that either Cys41 or Cys65 can bind Cu^{2+} to form a ~360 nm intermediate, but only the Cys41-Cu^{2+} 360 nm intermediate is used to form the Cu_A site. Thus, for the Cys65Ser variant, a greater amount of Cu_A is produced from a smaller amount of 360 nm intermediate as a result of less non-productive Cu^{2+} binding at the Cys65 site and more Cu^{2+} binding by Cys41.

Consistent with the notion that the faster-forming/decaying Cys65-Cu^{2+} 360 nm intermediate cannot convert to Cu_A, both the Met49Ala and His51Ala variants form a 360 nm intermediate that forms and decays on the same timescale as WT PmoD, yet neither produces a Cu_A (Figures 2D, E, Table S1). Thus, this intermediate species is not stable even when it does not convert to a Cu_A site. Mutation of both Cys residues prevents formation of both the 360 nm intermediate and Cu_A (Figure 2F), as expected since this variant does not bind copper. These data indicate that the PmoD Cu_A site forms via a modified version of the Cu_AAz "capture complex" mechanism, wherein Cys41 recruits Cu^{2+} for Cu_A formation.

PmoD Cu_A decays to type 2 mononuclear Cu centers. We also noticed that the PmoD Cu_A spectroscopic features decay slowly, on the timescale of hours at 4 °C under aerobic conditions (Figure 3A). All previously characterized Cu_A centers are quite stable at physiological pH, with the exception of a Cu_A site engineered into a coiled-coil scaffold that decayed over a time of approximately 6 hours.[30] The PmoD Cu_A center decays to form a species with no CT bands in the optical spectrum, only a broad Cu^{2+} d-d transition at ~615 nm (Figure 3A). The Cu_A decay was monitored over several days at 4 °C via optical and continuous wave (CW) X-band EPR spectroscopy for WT PmoD. The Cu_A site decayed into two distinct type 2 Cu^{2+} centers, as evidenced by the appearance of two overlapping but distinguishable Cu^{2+} EPR signals with g_z and A_z consistent with type 2 Cu^{2+} (Cu_1 $g_z = 2.23$, $A_z = 610$ MHz; Cu_2 $g_z = 2.20$, $A_z = 545$ MHz, Figure 3B, Table 1).

Concomitant with the aerobic loss of the Cu_A optical and EPR spectroscopic features, the concentration of paramagnetic Cu becomes almost three-fold higher (Figure 3A, B). As Cu_A-$[2Cu]^{3+}$ oxidation to two monocopper Cu^{2+} ions would at most double the concentration of paramagnetic Cu, the starting protein must also contain a substantial amount of mononuclear Cu^{+} or Cu_A-$[2Cu]^{2+}$, which air oxidizes. As WT PmoD binds more than one Cu equivalent per monomer,[7] this result indicates that some of this excess copper is mononuclear Cu^{+}.

Although the Cu_A site bridges the monomer-monomer interface, PmoD remains a dimer even after Cu_A decay, as determined by size exclusion chromatography of the Cys65Ser PmoD variant, which only has one Cys per monomer (Figure S1). This variant decays to the same type 2 Cu^{2+} centers as WT PmoD (Figure S2) indicating that the decay process is the same for WT and mutant.

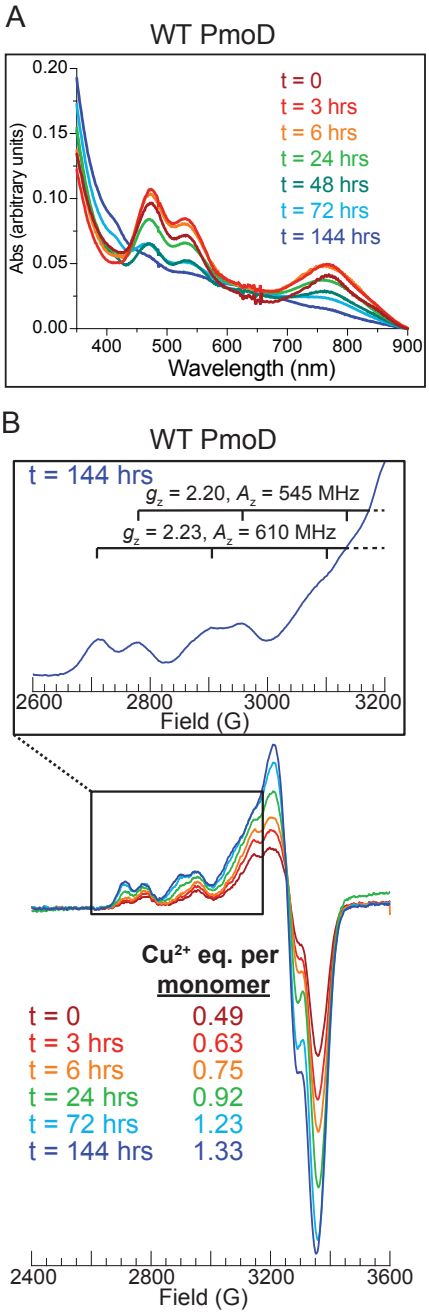

Figure 3. Decay of WT PmoD Cu_A at 4 °C observed in parallel by (A) optical and (B) CW X-band EPR spectroscopies. The inset in B depicts scans measured in the g_z region for the WT PmoD t = 144 hr sample, where brackets define the hyperfine splitting A_z of the two type 2 Cu^{2+} centers (the fourth hyperfine line is outside of the range shown). Conditions: (B inset) 9.364-9.365 GHz microwave frequency, 40 s scan rate, 320 ms time constant, 12.5 G modulation amplitude, temperature 20 K; (B bottom) 9.364-9.366 GHz microwave frequency, 90 s scan rate, 320 ms time constant, 12.5 G modulation amplitude, temperature 20 K. Spectra intensities were normalized to account for different gain settings. The protein concentration was 150 μM for all samples.

The Cys65Ser PmoD dimer post Cu_A decay is maintained after treatment with EDTA (to remove copper) in denaturing gel electrophoresis experiments performed under nonreducing conditions, but not under reducing conditions (Figure S1), indicating that an intermolecular disulfide bond links the two monomers. The disulfide must therefore be formed by the two Cys41 residues as Cys41 is the only cysteine residue present in Cys65Ser PmoD. Moreover, the Cys41Ser/Cys65Ser variant is exclusively monomeric (Figure S3). This conclusion is reminiscent of other studies that have reported Cu_A destruction with concomitant disulfide formation when attempting to oxidize the $[2Cu]^{3+}$ state.[1]

Table 1. PmoD paramagnetic spectroscopic features.

Paramagnet	g_x, g_y, g_z	*Cu* A_z *(MHz)*	$^{14}N_1$ $A_{x,y}$, A_z *(MHz)*§	$^{14}N_2$* $A_{x,y}$, A_z *(MHz)*§	*Cys-*C_β $^1H_1$ $A_{x,y}$, A_z▽ *(MHz)*	*Cys-*C_β $^1H_2$ $A_{x,y,z}$ *(MHz)*
Cu$_A$	2.01, 2.05, 2.13	141	+17, +16.5	+16, +16.5	+14.5, +17	~4.5
Type 2 Cu$_1$	-, -, 2.23	610				
Type 2 Cu$_2$	-, -, 2.20	545				

* $^{14}N_2$ shows resolved quadrupole splitting at the high field extreme, $3P = 2.3$ MHz.

§ ^{14}N hyperfine couplings assumed to be positive, as necessitated by the fact that they are directly-coordinated in-plane Cu ligands (with respect to the $Cu_2[S(Cys)]_2$ core).

▽ To determine the sign of $A_{Cys-C_\beta\ ^1H_1}$, we conducted pulsed ENDOR saturation recovery (PESTRE)[31] measurements (Figure S7). Such measurements indicate that for PmoD, $A_{Cys-C_\beta\ ^1H_1} > 0$, consistent with past characterization of other Cu_A centers.[21,32]

Nuclear magnetic resonance characterization of the PmoD Cu_A site. To further assess the differences between the PmoD Cu_A site and previously characterized Cu_A sites, we examined PmoD using NMR. NMR can be applied to proteins with fast relaxing paramagnets like Cu_A centers and provides a wealth of information on both the ligation of the Cu_A site and the presence of thermally-accessible excited electronic state(s). At room temperature, typical Cu_A centers are in dynamic equilibrium between two states, a majority form with a low energy σ_u* ground electronic state (GS) and a minority form with a π_u GS (Figure 4).[12,20,33,34] The two

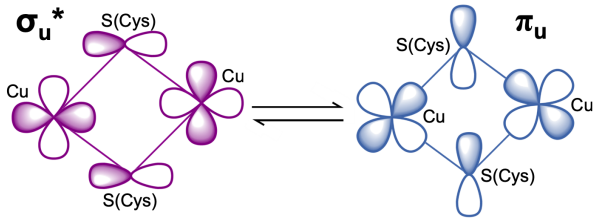

Figure 4. Schematic representation of the two alternative ground electronic states in the thermal equilibrium in typical Cu_A sites, σ_u* and π_u.

states are proposed to provide distinct electron transfer pathways for Cu_A reactivity in vivo.[20] In the typical Cu_A center, an equilibrium population of the π_u GS leads to fast overall electron-spin relaxation times (10^{-11} s) that produce sharp signals in the NMR spectra of Cu_A ligands with sharp resonances. Surprisingly, the ^1H NMR spectrum of PmoD instead showed a set of broad resonances (*a*-*e*) located between 50 and -10 ppm (Figure 5A). When the Cu_A site decays as discussed above, resonances *b*-*e* disappear, leaving only the broad signal *a*. Resonances *b*-*e* are thus attributed to the Cu_A center; signal *a*, which does not

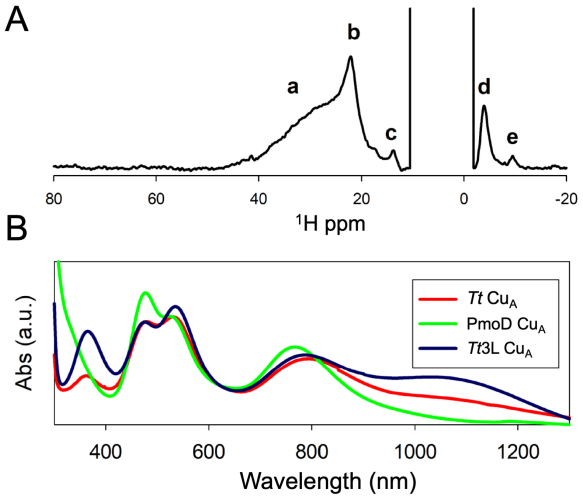

Figure 5. Paramagnetic NMR and electronic spectra suggest the absence of a thermally-accessible π_u state in the PmoD Cu_A. (A) 600 MHz ^1H NMR spectra of PmoD Cu_A recorded at 298 K in H_2O. The broad signal *a* is observed after loss of the purple color, and is therefore attributed to a different Cu^{2+} binding site. Resonances *b*-*e* correspond to copper ligands of the PmoD Cu_A site. (B) Optical spectrum of PmoD Cu_A compared to those of subunit II of *Tt* C*c*O *ba*$_3$ Cu_A and a loop mutant with a larger population of the π_u state, *Tt*3L Cu_A.[40]

correspond to the Cu_A center, is attributed to a distinct Cu^{2+} site. The loss of the Cu_A signals confirm that it converts to type 2 Cu^{2+} sites, whose slow electron-spin relaxation prevents observation of NMR signals from ligand nuclei.

The line widths of resonances *b-e* from the Cu_A center resemble those of oxidized type 1 blue copper centers, which exhibit longer electron relaxation times of 10^{-10} s,[35,36] and are much broader than those of other Cu_A sites. Since a 1% population of the π_u GS is enough to provide an efficient relaxation pathway giving sharp NMR lines,[20] we conclude that the π_u GS in PmoD Cu_A is not thermally accessible, in contrast to all other known Cu_A sites. This conclusion is supported by the temperature dependence of the contact-shifted resonances in the PmoD NMR spectrum. In typical Cu_A NMR spectra, the chemical shifts show temperature dependences with large deviation from the Curie law, an effect of relaxation associated with occupation of the π_u GS.[33,37] In contrast, the temperature dependences of all ^{1}H NMR resonances in PmoD Cu_A follow the Curie law, confirming that such a GS is not significantly populated (temperature dependence of isolatable signals *c* and *d* shown in Figure S4).

The conclusion from the NMR data that the PmoD Cu_A center has a pure σ_u* GS is also supported by optical spectroscopic characterization. The intensity ratio of the LMCT bands at 350 and 530 nm is another bona fide indicator of the relative population of these two GS,[38] and the absence of a band at *ca.* 350 nm in PmoD Cu_A, in contrast to other Cu_A sites (Figure 5B), supports a null population of the π_u level.

Finally, the unusually small g_z value observed in the PmoD Cu_A EPR spectrum is entirely consistent with the conclusions derived from the NMR results. The g_z values of Cu_A centers have been related to the energy gap between the σ_u* GS and the π_u Franck-Condon excited state (ES) according to the equation[34,39]

$$g_z \approx g_e + 8\zeta_{3d}^{Cu}\alpha^2\beta^2/\Delta_{\frac{\sigma_u^*}{\pi_u}} \quad (1)$$

in which g_e is the *g*-factor for a free electron, α^2 and β^2 represent the Cu character of the σ_u* and π_u states, respectively, and ζ_{3d}^{Cu} is the Cu^{2+} spin-orbit coupling constant for the 3d wave functions. By applying the parameters reported for other Cu_A centers[34] ($\alpha^2 = 0.44$, $\beta^2 = 0.33$) and the experimentally determined g_z value, we calculate an approximation of the energy gap between the σ_u* GS and a π_u ES as 6950 cm^{-1}, the largest of any known Cu_A center, consistent with the observed NMR features and null population of the π_u GS (Table S2).

ENDOR, ESEEM, and HYSCORE characterization of the PmoD Cu_A ligation sphere. Previous mutagenesis data implicated His51 in PmoD Cu_A formation.[7] To further investigate nitrogen ligation of the Cu_A site, we collected Q-band EPR (Figure 6A) and ^{14}N-ENDOR (Figure 6B) spectra to detect and characterize directly coordinated nitrogenous ligands.

Cu_A centers typically exhibit two strongly-coupled N(His) hyperfine couplings corresponding to the two N(His) ligands.[41-43] These N(His) hyperfine couplings (6 MHz $\lesssim$ Cu_A $A_{x,y,z}(^{14}N)$ $\lesssim$ 20 MHz) are substantially smaller than those of typical mononuclear Cu-N(His) ligands.[41-43] Orientation-selective Davies ENDOR spectra of PmoD Cu_A reveal the presence of an effectively isotropic, strongly-coupled ^{14}N ENDOR response with $A(^{14}N)$ ~ 16-17 MHz, arising from direct ligation of ^{14}N to the Cu_A (Figure 6B). Additional ^{14}N resonances observed at higher frequency are attributed to ^{14}N ligand(s) of the underlying mononuclear Cu^{2+} signal evident in the Q-band EPR spectrum (Figure 6A, Figure S5A).

Considering the number of ^{14}N ligands that contribute to the PmoD ENDOR response, the observation of a seven hyperfine line splitting pattern in the EPR spectrum of PmoD requires that the two Cu ions must be in essentially equivalent environments. Therefore, there cannot be only one directly coordinated N ligand, as it would produce a highly asymmetric ligand field and valence localization (i.e. the EPR spectrum would resemble a mononuclear Cu^{2+} spectrum with four resolved Cu hyperfine lines) as seen in the His120Ala Cu_AAz mutant.[11] Thus, the strongly-coupled ^{14}N ENDOR response is assigned to two Cu_A ^{14}N ligands with nearly identical, effectively isotropic hyperfine coupling, Table 1). This conclusion is consistent with the previous proposal that one His51 from each monomer in the Cu_A-containing PmoD homodimer serves as a ligand (Figure 1).[7] While it is possible to form a Cu_A center with only one His ligand,[11] Cu_A formation was not observed in the His51Ala PmoD variant,[7] necessitating assignment of both Cu_A N(His) ligands to His51 side chains.

The near equivalence of the two isotropic couplings suggests two nitrogenous ligands bound to PmoD Cu_A in a very symmetrical fashion. As expected, ESEEM and HYSCORE spectroscopy measurements identified two weakly-coupled ^{14}N nuclei (Figure S6) characteristic of the distal, non-coordinated nitrogen from two N(His) imidazole side chain ligands to the Cu_A. Thus, the two strongly-coupled, nearly identical ^{14}N ENDOR responses correspond to two directly coordinated N(His) Cu_A ligands. The isotropic component of the strongly-coupled ^{14}N hyperfine coupling (A_{iso} ~16-17 MHz for the two His) is proportional to the magnitude of ρ_N, and the sum of the two A_{iso} values is the largest of any Cu_A site characterized to date (Table S3). This implied additional delocalization in the PmoD Cu_A-N bonding is consistent with the optical spectroscopy, which also indicated enhanced ligand spin density relative to other Cu_A centers.

To further define the geometry of the PmoD Cu_A center, we examined past crystal structures and ENDOR studies of Cu_A-containing proteins to identify structural and spectroscopic correlation(s). We find that increasing colinearity of the two N(His)-Cu bond vectors of a Cu_A site with respect to the Cu-Cu vector correlates with increased sum of ^{14}N(His)-A_{iso} of the two ^{14}N(His) ligands (Table S3). Given the nearly identical hyperfine

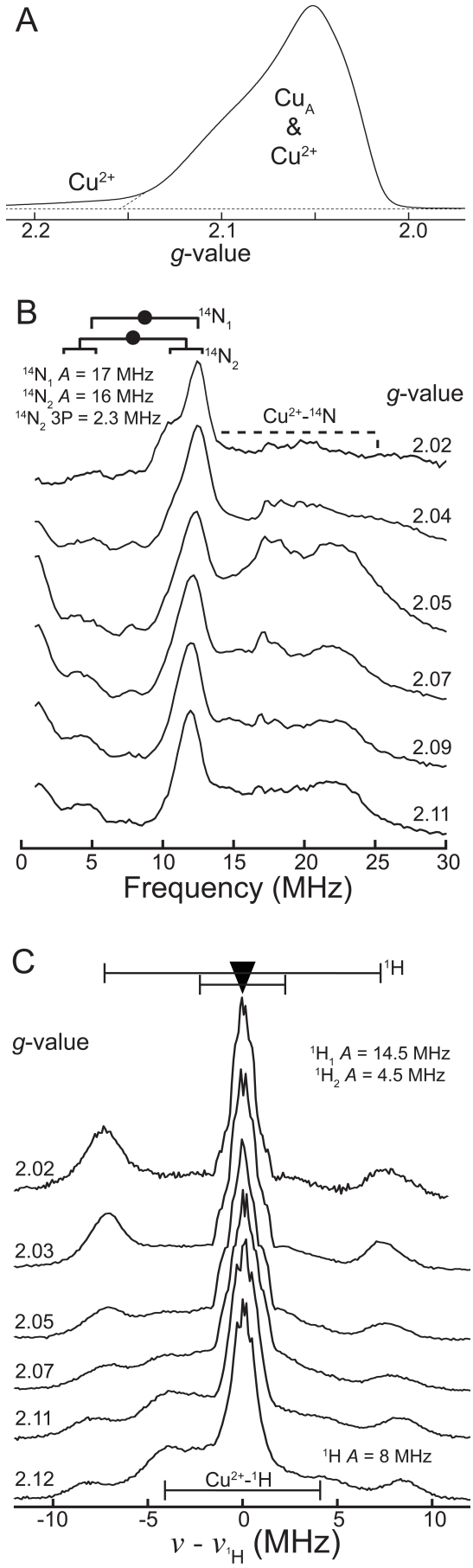

Figure 6. Pulsed Q-band two pulse EPR and ^{14}N, ^{1}H Davies ENDOR of PmoD. (A) Two pulse echo-detected EPR. The Cu^{2+} region denoted by the dotted line, $g \sim 2.2$-2.15, is attributable to exclusively mononuclear Cu^{2+} resonance, while the region from $g \sim 2.15 - 2.0$ corresponds to predominantly Cu_A resonance (as well as the overlapping minor Cu^{2+} resonance). Field-swept spectrum with X-axis of magnetic field provided in Figure S8. (B) ^{14}N Davies ENDOR measurements across the EPR envelope at *g*-values indicated, demonstrating the nearly equivalent hyperfine coupling of the two Cu_A ^{14}N ligands. The region under the dotted brackets denotes resonance attributable to Cu^{2+}-^{14}N ligation, as confirmed in Figure S5A. The black goalpost width signifies twice the ^{14}N Larmor frequency ($2 \times \nu_{^{14}N}$), and the filled circle denotes one half the ^{14}N hyperfine coupling ($A/2$). Additional splitting resolved at the high field edge ($g = 2.02$) of the $^{14}N_2$ resonance is attributed to resolved quadrupole splitting $3P = 2.3$ MHz. Only the higher frequency ν^+ peaks are well-resolved. (C) ^{1}H Larmor-centered Davies ENDOR, where the triangle denotes the ^{1}H Larmor frequency ($\nu_{^1H}$) and goalpost width defines the hyperfine coupling magnitude (A) to Cu_A Cys-C_β ^{1}H (black). The modestly large ^{1}H response seen at lower fields ($A \sim 8$ MHz) is attributed to a ^{1}H coupled to the underlying Cu^{2+} resonance, as confirmed in Figure S5B. EPR conditions: 34.649 GHz microwave frequency, 200 s scan, $\pi = 80$ ns, $\tau = 500$ ns, 20 ms repetition time; ^{14}N ENDOR conditions: 34.63-34.67 GHz microwave frequency, $\pi = 80$ ns, $\tau = 375$ ns, $T_{RF} = 200$ µs, 20 ms repetition time; ^{1}H ENDOR conditions: 34.64-34.65 GHz microwave frequency, $\pi = 200$ ns, $\tau = 575$ ns, $T_{RF} = 60$ µs, 50 ms repetition time.

couplings of the two N(His) ligands, and the fact that the sum of A_{iso} for the Cu_A ^{14}N(His) of PmoD is larger than for all previously characterized Cu_A centers, we deduce that the PmoD Cu_A His ligands coordinate the $Cu_2[S(Cys)]_2$ core in a very symmetrical fashion, with an essentially linear, N-Cu-Cu-N arrangement, strongly resembling Cu_AAz.[6]

We also characterized the two proposed S(Cys41) components of the $Cu_2[S(Cys)]_2$ core by ENDOR. Cu_A Cys ligands exhibit large isotropic hyperfine couplings to the Cys-C_β ^{1}H that arise from hyperconjugation to, and are proportional to, the magnitude of the spin density on the S(Cys). In the PmoD Cu_A ^{1}H ENDOR spectrum (Figure 6C), there are two well-resolved ^{1}H responses that do not exchange in D_2O (Figure S9) and exhibit large, isotropic coupling consistent with a Cu_A Cys-C_β ^{1}H: $A_{\text{iso Cys}-C_\beta\ ^1H_1} = 15$ MHz and $A_{\text{iso Cys}-C_\beta\ ^1H_2} \approx 4.5$ MHz (Table 1). The $A_{\text{iso Cys}-C_\beta\ ^1H_1} = 15$ MHz, and thus the spin density on S(Cys41), is similar to the largest reported to date for a Cu_A (Cu_A-containing soluble fragment of *Tt* C*c*O *ba*$_3$, Cu_A Cys-C_β ^{1}H $A_{iso\ max} = 15.4$ MHz, where total $\rho_{S(Cys)} = \sim 50$-55%).[21]

DISCUSSION

We here provide an extensive spectroscopic characterization of the formation and characteristics of the PmoD Cu_A, finding both similarities and key differences relative to other Cu_A centers. Stopped-flow optical spectroscopy indicates that, like Cu_AAz, the PmoD Cu_A forms via a cysteine "capture complex" mechanism, in which a solvent exposed cysteine (Cys41) binds and positions the Cu for Cu_A formation. However, unlike all other biological or semisynthetic Cu_A centers, the PmoD Cu_A is unstable, in the presence of air slowly decaying to two type 2 Cu^{2+} centers. Moreover, through NMR we have shown that the PmoD Cu_A is unlike all other Cu_A centers in that in fluid solution it exclusively resides in a form that features a σ_u* GS without a contribution from a form with π_u GS. Finally, advanced paramagnetic resonance characterization of the PmoD Cu_A and Cu_A ligands interpreted in the context of past work[7] confirmed (1) that two His51 side chains ligate the Cu_A and (2) the Cu_A ligands feature anomalously large spin density relative to what would be expected from interpreting the optical spectroscopy (and particularly the similarity of the spectrum to Cu_AAz).

In addition to the two S(Cys41) and two symmetrically-placed N(His51) ligands, the ligation sphere of the PmoD Cu_A site is likely completed by two axial Met49 thioethers.[7] Indeed, the observed spectroscopic characteristics of the PmoD Cu_A site are readily rationalized by considering the contributions for the two Met axial ligands. For previously characterized Cu_A sites, stronger axial ligation extends the Cu-Cu distance, weakening Cu-Cu and Cu-N(His) bonding while shifting spin density from the ligands onto the Cu.[44,45] Conversely, weaker axial ligation shortens the Cu-Cu distance by strengthening Cu-Cu bonding.[46] Furthermore, as a general rule, hard Lewis base axial Cu_A ligands bind more strongly than soft ones. Consequently, substitution of the typical Cu_A axial carbonyl ligand with the S of a Met side chain, which is a softer Lewis base, should increase ligand spin density at the expense of Cu spin density, and result in a very short Cu-Cu distance. Thus, the apparent discrepancy between the PmoD Cu_A and Cu_AAz optical and paramagnetic resonance properties, namely the failure of similar energies for the near-IR intervalence CT bands to correspond to similar spin density distributions, is rationalized as follows: the proteins both have strong Cu-Cu bonding and a short Cu-Cu distance, hence the same near-IR transition energy, but the two weak S(Met) ligands in PmoD Cu_A support increased covalency with the N(His) and S(Cys) ligands. This increased covalency causes PmoD to exhibit very small Cu_A A_z and ρ_{Cu} combined with large ligand hyperfine couplings and large ligand spin densities. In addition, in Cu_AAz, mutation of Met to stronger axial ligands decreases $\Delta_{\frac{\sigma_u^*}{\pi_u}}$.[12,20] Following this trend, the two weak axial Met ligands in PmoD are expected to increase the value of $\Delta_{\frac{\sigma_u^*}{\pi_u}}$, consistent with the fact that the PmoD $\Delta_{\frac{\sigma_u^*}{\pi_u}}$ value is the largest of any Cu_A.

A symmetrical Cu_A site (D_{2h} symmetry) with equivalent Met ligands would dramatically lower the intensity of the 530 nm S(Cys) to Cu LMCT band because this transition would be Laporte-forbidden.[12] Due to the instability of the site, we could not determine extinction coefficients for the PmoD Cu_A optical features. Instead, the 475 nm LMCT band intensity is much less sensitive to changes in axial ligation,[12] and consequently the intensity of the 530 nm LMCT band relative to the 475 nm LMCT band may be used as a surrogate for the 530 nm extinction coefficient. The ratio of 530 nm to 475 nm intensities is lower for PmoD Cu_A than for any other biological or engineered Cu_A (0.81 in PmoD, compared to 0.90 in Cu_AAz, 1.02 in N_2OR, and 1.03 in C*c*O),[1] indicating a very symmetrical site. However, the presence of a prominent 530 nm LMCT band indicates that the axial Met ligands do not bind the Cu_A equivalently and/or other noncovalent interaction(s) with the Cu_A center cause distortion from perfect symmetry.

PmoD is needed for copper-dependent growth of methanotrophs, but its specific function remains unknown.[7] It is not clear whether the Cu_A site is formed in vivo when PmoD is tethered to the inner membrane or whether the site itself is linked to the observed growth defect in the absence of PmoD.[7] However, it is tempting to speculate that PmoD is involved in electron transfer (ET) to pMMO, perhaps reducing the catalytic Cu center. If PmoD does shuttle electrons to an oxidant, its unique Cu_A site may offer some advantages. The π_u GS has larger inner and outer sphere reorganization energies than the σ_u* GS;[34,38] thus by not accessing the π_u GS, the PmoD Cu_A would lower ET reorganization energy, resulting in faster ET. Additionally, in the C*c*O Cu_A, there are distinct ET pathways from the Cu_A center through both the S(Cys) and N(His) ligands to the target heme.[3,12,20,34] In this way, ET may thus be optimized for a σ_u* GS. While additional work is needed to address how the unprecedented electronic structure of the PmoD Cu_A site relates to biological function, the current results show that it significantly expands the diversity of known Cu_A sites.

ASSOCIATED CONTENT

Supporting Information. Size exclusion chromatography traces and nondenaturing gel electrophoresis probing the dimeric nature of the post-Cu_A-decay PmoD, optical and spectroscopic monitoring of the Cys65Ser PmoD Cu_A decay, ENDOR comparison of Cu_A resonance compared to on overlapping monocopper Cu^{2+} resonance, ESEEM and HYSCORE characterization of distal imidazole ^{14}N from Cu_A-N(His) ligands, 1H ENDOR in H_2O vs. D_2O buffer, presentation of Q-band EPR with magnetic field as x-axis, PESTRE $A_{Cys-C_\beta\ ^1H}$ sign determination, stopped flow kinetics parameters, geometry and ^{14}N isotropic hyperfine couplings from various Cu_A centers. The Supporting Information is available free of charge on the ACS Publications website.

AUTHOR INFORMATION

Corresponding Author

*To whom correspondence should be addressed: (B.M.H.) bmh@northwestern.edu, (A.C.R.) amyr@northwestern.edu

Author Contributions

§M.O.R. and O.S.F. contributed equally to this work.

Funding Sources

This work was supported by Department of Energy grant DE-SC0016284 (A.C.R.), National Institutes of Health Award grants GM111097 (B.M.H.), 5T32GM008382 (M.O.R.), and F32GM119191 (O.S.F.), and Department of Energy grant DE-FG02-99ER14999 (M.R.W.). M.N.M is recipient of a postdoctoral fellowship from CONICET and A.J.V. is staff member from CONICET. The Quantitative Bio-element Imaging Center at Northwestern is supported by NASA Ames Research Center NNA06CB93G. The Keck Biophysics Facility at Northwestern is supported in part by NCI CCSG P30 CA060553.

Notes

No competing financial interests have been declared.

ACKNOWLEDGMENT

We thank Profs. Laura M. K. Dassama and Yi Lu for helpful discussions.

REFERENCES

(1) Liu, J.; Chakraborty, S.; Hosseinzadeh, P.; Yu, Y.; Tian, S.; Petrik, I.; Bhagi, A.; Lu, Y. *Chem. Rev.* **2014**, *114*, 4366.

(2) Beinert, H. *Eur. J. Biochem.* **1997**, *245*, 521.

(3) Solomon, E. I.; Xie, X.; Dey, A. *Chem. Soc. Rev.* **2008**, *37*, 623.

(4) Williams, P. A.; Blackburn, N. J.; Sanders, D.; Bellamy, H.; Stura, E. A.; Fee, J. A.; McRee, D. E. *Nat. Struct. Mol. Biol.* **1999**, *6*, 509.

(5) Brown, K. R.; Djinovic-Carugo, K.; Haltia, T.; Cabrito, I.; Saraste, M.; Moura, J. J. G.; Moura, I.; Tegoni, M.; Cambillau, C. *J. Biol. Chem.* **2000**, *275*, 41133.

(6) Robinson, H.; Ang, M. C.; Gao, Y.-G.; Hay, M. T.; Lu, Y.; Wang, A. H.-J. *Biochemistry* **1999**, *38*, 5677.

(7) Fisher, O. S.; Kenney, G. E.; Ross, M. O.; Ro, S. Y.; Lemma, B. E.; Batelu, S.; Thomas, P. M.; Sosnowski, V. C.; DeHart, C. J.; Kelleher, N. L.; Stemmler, T. L.; Hoffman, B. M.; Rosenzweig, A. C. *Nat. Commun.* **2018**, *9*, 4276.

(8) Sirajuddin, S.; Rosenzweig, A. C. *Biochemistry* **2015**, *54*, 2283.

(9) Kenney, G. E.; Sadek, M.; Rosenzweig, A. C. *Metallomics* **2016**, *8*, 931.

(10) DeBeer George, S.; Metz, M.; Szilagyi, R. K.; Wang, H.; Cramer, S. P.; Lu, Y.; Tolman, W. B.; Hedman, B.; Hodgson, K. O.; Solomon, E. I. *J. Am. Chem. Soc.* **2001**, *123*, 5757.

(11) Xie, X.; Gorelsky, S. I.; Sarangi, R.; Garner, D. K.; Hwang, H. J.; Hodgson, K. O.; Hedman, B.; Lu, Y.; Solomon, E. I. *J. Am. Chem. Soc.* **2008**, *130*, 5194.

(12) Tsai, M.-L.; Hadt, R. G.; Marshall, N. M.; Wilson, T. D.; Lu, Y.; Solomon, E. I. *Proc. Natl. Acad. Sci.* **2013**, *110*, 14658.

(13) Slutter, C. E.; Gromov, I.; Richards, J. H.; Pecht, I.; Goldfarb, D. *J. Am. Chem. Soc.* **1999**, *121*, 5077.

(14) Hay, M. T.; Ang, M. C.; Gamelin, D. R.; Solomon, E. I.; Antholine, W. E.; Ralle, M.; Blackburn, N. J.; Massey, P. D.; Wang, X.; Kwon, A. H. *Inorg. Chem.* **1998**, *37*, 191.

(15) Prudêncio, M.; Pereira, A. S.; Tavares, P.; Besson, S.; Cabrito, I.; Brown, K.; Samyn, B.; Devreese, B.; Van Beeumen, J.; Rusnak, F.; Fauque, G.; Moura, J. J. G.; Tegoni, M.; Cambillau, C.; Moura, I. *Biochemistry* **2000**, *39*, 3899.

(16) Slutter, C. E.; Sanders, D.; Wittung, P.; Malmström, B. G.; Aasa, R.; Richards, J. H.; Gray, H. B.; Fee, J. A. *Biochemistry* **1996**, *35*, 3387.

(17) Hay, M.; Richards, J. H.; Lu, Y. *Proc. Natl. Acad. Sci.* **1996**, *93*, 461.

(18) Blackburn, N. J.; de Vries, S.; Barr, M. E.; Houser, R. P.; Tolman, W. B.; Sanders, D.; Fee, J. A. *J. Am. Chem. Soc.* **1997**, *119*, 6135.

(19) Charnock, J. M.; Dreusch, A.; Körner, H.; Neese, F.; Nelson, J.; Kannt, A.; Michel, H.; Garner, C. D.; Kroneck, P. M.; Zumft, W. G. *Eur. J. Biochem.* **2000**, *267*, 1368.

(20) Abriata, L. A.; Álvarez-Paggi, D.; Ledesma, G. N.; Blackburn, N. J.; Vila, A. J.; Murgida, D. H. *Proc. Natl. Acad. Sci.* **2012**, *109*, 17348.

(21) Epel, B.; Slutter, C. S.; Neese, F.; Kroneck, P. M. H.; Zumft, W. G.; Pecht, I.; Farver, O.; Lu, Y.; Goldfarb, D. *J. Am. Chem. Soc.* **2002**, *124*, 8152.

(22) Komorowski, L.; Anemüller, S.; Schäfer, G. *J. Bioenerg. Biomembr.* **2001**, *33*, 27.

(23) Inubushi, T.; Becker, E. D. *J. Magn. Reson.* **1983**, *51*, 128.

(24) Davoust, C. E.; Doan, P. E.; Hoffman, B. M. *J. Magn. Reson. A* **1996**, *119*, 38.

(25) Epel, B.; Gromov, I.; Stoll, S.; Schweiger, A.; Goldfarb, D. *Concepts Magn. Reson. Part B Magn. Reson. Eng.* **2005**, *26*, 36.

(26) Savelieff, M. G.; Wilson, T. D.; Elias, Y.; Nilges, M. J.; Garner, D. K.; Lu, Y. *Proc. Natl. Acad. Sci.* **2008**, *105*, 7919.

(27) Wilson, T. D.; Savelieff, M. G.; Nilges, M. J.; Marshall, N. M.; Lu, Y. *J. Am. Chem. Soc.* **2011**, *133*, 20778.

(28) Chakraborty, S.; Polen, M. J.; Chacón, K. N.; Wilson, T. D.; Yu, Y.; Reed, J.; Nilges, M. J.; Blackburn, N. J.; Lu, Y. *Biochemistry* **2015**, *54*, 6071.

(29) Chacón, K. N.; Blackburn, N. J. *J. Am. Chem. Soc.* **2012**, *134*, 16401.

(30) Shiga, D.; Funahashi, Y.; Masuda, H.; Kikuchi, A.; Noda, M.; Uchiyama, S.; Fukui, K.; Kanaori, K.; Tajima, K.; Takano, Y. *Biochemistry* **2012**, *51*, 7901.

(31) Doan, P. E. *J. Magn. Reson.* **2011**, *208*, 76.

(32) Epel, B.; Manikandan, P.; Kroneck, P. M. H.; Goldfarb, D. *Appl. Magn. Reson.* **2001**, *21*, 287.

(33) Abriata, L. A.; Ledesma, G. N.; Pierattelli, R.; Vila, A. J. *J. Am. Chem. Soc.* **2009**, *131*, 1939.

(34) Gorelsky, S. I.; Xie, X.; Chen, Y.; Fee, J. A.; Solomon, E. I. *J. Am. Chem. Soc.* **2006**, *128*, 16452.

(35) Bertini, I.; Fernández, C. O.; Karlsson, B. G.; Leckner, J.; Luchinat, C.; Malmström, B. G.; Nersissian, A. M.; Pierattelli, R.; Shipp, E.; Valentine, J. S.; Vila, A. J. *J. Am. Chem. Soc.* **2000**, *122*, 3701.

(36) Donaire, A.; Jiménez, B.; Fernández, C. O.; Pierattelli, R.; Niizeki, T.; Moratal, J.-M.; Hall, J. F.; Kohzuma, T.; Hasnain, S. S.; Vila, A. J. *J. Am. Chem. Soc.* **2002**, *124*, 13698.

(37) Bertini, I.; Bren, K. L.; Clemente, A.; Fee, J. A.; Gray, H. B.; Luchinat, C.; Malmström, B. G.; Richards, J. H.; Sanders, D.; Slutter, C. E. *J. Am. Chem. Soc.* **1996**, *118*, 11658.

(38) Zitare, U.; Alvarez-Paggi, D.; Morgada, M. N.; Abriata, L. A.; Vila, A. J.; Murgida, D. H. *Angew. Chem.* **2015**, *127*, 9691.

(39) Neese, F.; Zumft, W. G.; Antholine, W. E.; Kroneck, P. M. *J. Am. Chem. Soc.* **1996**, *118*, 8692.

(40) Morgada, M. N.; Abriata, L. A.; Zitare, U.; Alvarez-Paggi, D.; Murgida, D. H.; Vila, A. J. *Angew. Chem.* **2014**, *126*, 6302.

(41) Lukoyanov, D.; Berry, S. M.; Lu, Y.; Antholine, W. E.; Scholes, C. P. *Biophys. J.* **2002**, *82*, 2758.

(42) Gurbiel, R. J.; Fann, Y. C.; Surerus, K. K.; Werst, M. M.; Musser, S. M.; Doan, P. E.; Chan, S. I.; Fee, J. A.; Hoffman, B. M. *J. Am. Chem. Soc.* **1993**, *115*, 10888.

(43) Neese, F.; Kappl, R.; Hüttermann, J.; Zumft, W.; Kroneck, P. *J. Biol. Inorg. Chem.* **1998**, *3*, 53.

(44) Slutter, C. E.; Gromov, I.; Epel, B.; Pecht, I.; Richards, J. H.; Goldfarb, D. *J. Am. Chem. Soc.* **2001**, *123*, 5325.

(45) Ledesma, G. N.; Murgida, D. H.; Ly, H. K.; Wackerbarth, H.; Ulstrup, J.; Costa-Filho, A. J.; Vila, A. J. *J. Am. Chem. Soc.* **2007**, *129*, 11884.

(46) Clark, K. M.; Tian, S.; van der Donk, W. A.; Lu, Y. *Chem. Commun.* **2017**, *53*, 224.

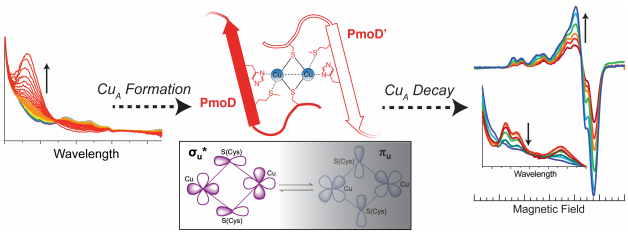

For Table of Contents Only